Sustainable Food Technology

ROYAL SOCIETY OF CHEMISTRY

PAPER

View Article Online
View Journal

Cite this: DOI: 10.1039/d5fb00795j

Effect of microbial transglutaminase crosslinking time on the structural, physicochemical and gelling properties of black soldier fly larvae protein: a texturization strategy for sustainable alternative proteins

Xin Yun Chia, [a] Siau Hui Mah [a] and Yun Ping Neo *[b]

Growing population pressures and envionmental concerns over conventional proteins have driven interest in sustainable alternatives such as black soldier fly larvae (BSFL) for texturized insect-based foods. However, the utilization of BSFL protein in food applications is limited and requires an understanding of its structural and functional properties, as well as the effects of processing conditions. This study investigates the effect of microbial transglutaminase (MTG)-catalysed crosslinking on the structural, physicochemical and gelling properties of BSFL protein. BSFL protein dispersions were subjected to different incubation times, ranging from 0.5 h to 24 h to achieve varying degrees of crosslinking. The results showed a consistent increase in the crosslinking degree with incubation time, with the highest level attained after 24 h. The progressive crosslinking of BSFL protein increased particle size but a smaller-sized population emerged after prolonged incubation for 20 h and 24 h. SDS-PAGE showed that 0.5 h to 24 h of MTG treatment resulted in the formation of high molecular weight aggregates (>250 kDa). Progressive reduction in sulfhydryl content and surface hydrophobicity with increasing incubation time indicates that MTG-induced crosslinking caused burial of sulfhydryl groups and hydrophobic residues within the protein network. FTIR analysis revealed that MTG-treated samples exhibit higher β-sheet content, suggesting structural reorganisation towards a more ordered conformation upon MTG-induced crosslinking. Functionally, MTG incubation time for 20 h yielded a BSFL protein network with the highest gel strength and water holding capacity. Extended incubation for 24 h started to compromise the gel strength and WHC. Overall, this study highlights the time-dependent nature of MTG-induced structural modifications and the gelling mechanism. It is important for laying the groundwork for manipulating the gelling properties of BSFL protein and the development of texturized BSFL protein-based insect-based foods, which could advance the utilisation of BSFL protein as a sustainable alternative protein.

Received 30th October 2025
Accepted 10th June 2026

DOI: 10.1039/d5fb00795j

rsc.li/susfoodtech

Sustainability spotlight

Black soldier fly larvae (BSFL) represent a promising alternative protein source due to their high bioconversion efficiency, nutritional value and lower ecological impacts compared to traditional livestock. This study utilized microbial transglutaminase (MTG) to promote BSFL protein crosslinking, enabling targeted modifications of protein structures and the improvement of gelation properties under mild processing conditions. This green and clean-label processing route offers an alternative to conventional protein structuring methods for the development of functional protein ingredients from a sustainable source. This aligns with the United Nations Sustainable Development Goals (SDGs) including SDG 2 (Zero Hunger), SDG 9 (Industry, Innovation and Infrastructure) and SDG 12 (Responsible Consumption and Production).

1 Introduction

The imperative to search for alternative and sustainable protein sources has garnered significant attention in recent years due to growing global demand for food and the environmental concerns related to conventional protein production.[1,2] Edible insects are reckoned as an underexploited yet promising protein source due to their low environmental footprint, high protein quality, rapid growth cycle, simple habitat and nutritional requirements.[3]

Black soldier fly larvae (BSFL, *Hermetia illucens*) have an edge over other edible insects due to their high feed conversion efficiency, strong survival rates and ability to digest a wide range

[a]School of Biosciences, Faculty of Health and Medical Sciences, Taylor's University, 47500, Subang Jaya, Selangor, Malaysia
[b]School of Hospitality and Tourism Management, Sunway University, 47500, Subang Jaya, Selangor, Malaysia. E-mail: yunpingn@sunway.edu.my

of organic substrates.[4–6] Specifically, the lower feed-conversion-ratio (FCR) of BSFL, in the range of 1.4–2.6, as compared to the higher FCR values reported for conventional protein sources such as poultry (2.3), pork (4.0) and beef (8.8) indicates that BSFL convert their feed into biomass more efficiently.[6,7] Meanwhile, these authors also found that the higher survival rate of BSFL was due to their lower sensitivity to variations in diet composition compared with other insects like crickets and mealworms. Due to the presence of a unique combination of digestive enzymes and gut microbiome, BSFL have been reported to feed on a variety of low-value, nutritionally poor organic materials, including food processing by-products such as spent grains, spent coffee, coconut endosperm, soybean curd, sweet potato peels, banana peels and general food waste.[4,5] These attributes make BSFL a highly sustainable protein source. At present, BSFL are one of the most commonly reared insect species on a commercial scale, with their applications confined to animal feed production and as a biotechnological tool for organic waste management.[5,8] Although BSFL show a promising nutritional profile and environmental sustainability benefits as an alternative protein source,[8–11] their use in food applications remains at an early stage of development, with current efforts limited to experimental formulations and pilot-scale studies.[12–15]

While utilizing insects including BSFL as a source of functional protein ingredients is a viable strategy to increase their use in food,[16] the limited understanding of the structural and functional properties of BSFL protein and how these properties are affected by processing conditions has become a major bottleneck in further expanding their applications.[17,18] Gelation is a key functional property of protein that plays an important role in rendering the structure and texture of many food systems. However, the gelling behaviour of BSFL protein remains largely underexplored, constraining the development of novel, structured food products.[19,20]

Enzymatic crosslinking using microbial transglutaminase (MTG, EC 2.3.2.13) represents an attractive, clean-label strategy to engineer protein gelling properties. MTG catalyses the acyl transfer reaction between the ε-amino of lysine and γ-amide of glutamine in proteins, resulting in formation of strong, irreversible ε-(γ-glutamyl)–lysine (G–L) covalent isopeptide bonds. These bonds facilitate inter- and/or intra-molecular protein crosslinking and promote the formation of a highly stable gel.[21] The high substrate specificity and mild reaction conditions of MTG enable controlled and targeted structural modification, providing a safer and eco-friendly method while overcoming the potential off-flavours development, nutrient degradation during thermal processing and toxicity concerns associated with other chemical crosslinkers.[22,23] Since MTG has been granted generally recognized as safe (GRAS) status by FAO, MTG has been widely used in the food industry to enhance texture and functionality of various protein systems, such as restructured meat, surimi, yoghurt, tofu, and cheese.[24–29]

Recent studies have also demonstrated the ability of MTG to crosslink proteins derived from edible insects and improve their functionality.[30,31] However, differences in the structural and compositional characteristics of insect proteins across species necessitate further investigation of the specific protein system of interest. Notwithstanding the fact that BSFL protein is a promising candidate for MTG crosslinking, given its richness in MTG substrates lysine and glutamine,[9,10,32] no study has yet investigated the susceptibility of BSFL protein to MTG-catalysed crosslinking or examined how such enzymatic modification affects its structural and gelation properties to date.

Hence, the present study aimed to systematically investigate the effect of MTG on the structural, physicochemical and gelation properties of BSFL protein over varying incubation times. It is hypothesized that incubation time modulates the extent of protein crosslinking, thereby influencing the protein's structure, aggregation and gelation behaviour. While our previous work demonstrated that gelation of BSFL protein using conventional heat treatment relies on temperature-dependent protein unfolding and aggregation,[33] the novelty of the present study lies in the investigation of BSFL protein gelation behaviour through site-specific ε-(γ-glutamyl)–lysine covalent crosslinking catalysed by MTG, a mechanistic pathway that has not been previously characterised in BSFL protein. Other than contributing new insights into the structural and physicochemical changes associated with MTG-mediated gel network formation, the findings from this study also serve as a useful reference for future development of texturized insect-based food products requiring milder processing conditions.

2 Materials and methods

2.1. Materials

Defatted BSFL powder was sourced from Life Origins Sdn. Bhd. (Seri Kembangan, Malaysia). The BSFL were reared in a controlled environment and fed on clean, standardised, traceable pre-consumer materials such as soybean meal, and coconut husk before harvest. The harvested BSFL were washed, blanched at 90 °C and air dried. Then, the dried BSFL were ground into powder and defatted using a proprietary mechanical heat pressing process at approximately 150 °C to 180 °C. However, the procedural details remain undisclosed due to commercial confidentiality. The defatted BSFL powder was used as the raw material for the extraction of BSFL protein using the alkali-solubilisation–acid-precipitation method detailed in our previous study.[33] The extracted BSFL protein, referred to as BSFL protein concentrate, was reported to contain 61.44% protein, 4.22% fat, 3.03% ash, 6.02% moisture and 25.29% carbohydrate.

MTG (SAE0159, Sigma-Aldrich, USA) was reconstituted according to the manufacturer's instructions by dissolving the lyophilized MTG with 1 mL of buffer containing 20 mM Tris–HCl and 150 mM NaCl at pH 8. The enzyme activity of MTG used in this study was 38 U mg^{-1} protein as determined using the hydroxamate assay, where one unit of MTG catalyses the formation of 1.0 μmol of hydroxamate per minute from the substrates NZ-Gln-Gly and hydroxylamine at pH 6.0 at 37 °C. The reconstituted stock solution was aliquoted and stored at −20 °C to avoid repeated freeze–thaw cycles. All chemical reagents used in this study were of analytical grade. Deionised

water was used for the preparation of solutions throughout the present study unless otherwise stated.

2.2. MTG crosslinking of samples

2.2.1. Preparation of protein dispersions. BSFL protein dispersions were prepared by dispersing the BSFL protein concentrate in 0.01 M phosphate buffer (pH 7). Protein dispersions at two different concentrations were prepared: 2% (w/v, protein basis) protein dispersions for structural and physicochemical property analyses; and 10% (w/v, protein basis) protein dispersions for evaluating the gelling properties. This approach ensures measurement compatibility for different analytical techniques and both the structural transitions occurring at the molecular level and bulk functional behaviour are captured.[34–38] Sodium azide was added at 0.02% w/v to inhibit microbial growth. The protein dispersions were then homogenized, stirred for 1 h at room temperature and allowed to hydrate overnight at 4 °C prior to subsequent treatments.

2.2.2. MTG treatment. BSFL protein dispersions were aliquoted and preheated at 37 °C for 10 min as an equilibration step before the addition of MTG. For sequential enzymatic reaction, MTG was added into the protein dispersions at a concentration of 5 U per g protein, followed by incubation at 37 °C for different time (0.5 h, 1 h, 2 h, 4 h, 20 h and 24 h) in an incubator (IN 110, Memmert, Germany). The enzyme concentration and incubation periods were selected based on the effective range of MTG reaction conditions commonly used for catalysing protein gelation.[39–42] At the end of each time point, the enzymatic reactions were terminated by immediately heating the samples to 85 °C for 5 min followed by rapid cooling in an ice bath. A control sample without the addition of MTG, referred to as non-MTG, was subjected to the same conditions to account for thermal effects.

2.3. Structural and physicochemical properties

2.3.1. Particle size and polydispersity index (PdI). The *z*-average (intensity-based mean hydrodynamic diameter), volume-based particle size distribution and PdI were determined using the dynamic light scattering (DLS) method with a zetasizer (Zetasizer Nano, Malvern Panalytical, UK). Prior to measurement, samples were diluted to 0.1% w/v using 0.01 M phosphate buffer (pH 7.0) to minimize multiple scattering and filtered through 0.45 μm cellulose acetate (CA) syringe filters to remove dust and large particulates. CA filters were used due to their low protein-binding properties that minimized sample loss during filtration. Next, the sample was transferred into a disposable cuvette and then thermally equilibrated at 25 °C for 120 s in the measurement cell. All DLS measurements were conducted using a backscattering angle of 173°, with the dispersant refractive index set at 1.33 and the particle refractive index set at 1.45. The volume-based particle size distributions were converted from the intensity-based distribution *via* Mie theory.

2.3.2. Turbidity. Turbidity of the MTG-treated BSFL protein dispersions was determined using a UV-Vis spectrophotometer (Genesys 10uv, Thermo Scientific, USA). Samples were diluted to 0.1% w/v using 0.01 M phosphate buffer (pH 7.0) before measurement. The diluted dispersions were gently mixed prior to reading to ensure homogeneity. Absorbance was recorded at 400 nm and 600 nm to enhance sensitivity for the detection of small and large particles, respectively.[43] Measurements were performed in a quartz cuvette at room temperature with deionised water serving as a blank for background correction.

2.3.3. Zeta potential. Zeta potential of BSFL protein dispersions was measured using a zetasizer (Zetasizer Nano, Malvern Panalytical, UK) to analyse the surface charge characteristics of the protein. Samples were prepared as described for particle size analysis and loaded into folded capillary cells (DTS 1070). Before measurement, the samples were equilibrated for 120 s at 25 °C. The dispersant properties were set as follows: a refractive index of 1.33, a dielectric constant of 78.5 and a viscosity of 0.887 mPa s. Electrophoretic mobility values were obtained and automatically converted to zeta potential values using the Smoluchowski model. The reported zeta potential value represents the average of five consecutive measurements with a 60 s delay between successive measurements, and each measurement consisted of 14 runs.

2.3.4. Free amino group content. To determine the degree of protein crosslinking, the relative change in free amino group content in MTG-treated BSFL protein dispersions was determined using *o*-phthaldialdehyde (OPA) method according to Hu *et al.* (2021)[44] with slight modifications. The OPA reagent was freshly prepared by dissolving 40 mg of OPA in 1 mL of methanol, followed by the addition of 2.5 mL of 20% (w/w) sodium dodecyl sulfate (SDS), 25 mL of 0.1 M sodium tetraborate (pH 9), and 100 μL of 2-mercaptoethanol (β-ME). The solution was then diluted to a final volume of 50 mL using deionized water. MTG-treated BSFL protein dispersions were centrifuged at 4000×*g* for 10 min at 4 °C using a microcentrifuge (5425R, Eppendorf, Germany). The supernatant was collected and diluted to 0.1% w/v. Approximately 400 μL of the diluted supernatants were mixed gently with 2 mL of the OPA reagent in a quartz cell individually, maintaining a sample-to-reagent-volume ratio of 1 : 5. After standing for 2 min at ambient temperature, the absorbance of the mixtures was measured immediately at 340 nm using a UV-vis spectrophotometer (Genesys 10uv, Thermo Scientific, USA) against a blank that consisted of phosphate buffer and OPA reagent only. Based on the reaction mechanism of MTG, the reduction in absorbance values was used to estimate the degree of crosslinking using the following equation.

$$\text{Crosslinking degree (\%)} = [1 - (A_{\text{modified}}/A_{\text{control}})] \times 100$$

Where A_{modified} and A_{control} represent the absorbance values of MTG-treated and untreated samples, respectively.

2.3.5. Sulfhydryl group (SH) content. The free and total SH contents were estimated using the methods described by Beveridge *et al.* (1974)[45] and Shen *et al.* (2017)[46] with slight modifications. For the determination of free SH, 0.5 mL of each sample was mixed with 2.5 mL of reaction buffer consisting of 0.1 M phosphate buffer (pH 8.0) containing 4 mM EDTA, and 50 μL of Ellman's reagent (4 mg mL^{-1} 5-5′-dithiobis(2-nitrobenzoic

acid), DTNB, in phosphate buffer, pH 8.0). For the determination of total SH content, the method was similar to the above, except that the reaction buffer additionally contained 8 M urea and was added under a nitrogen atmosphere. The reaction mixtures were incubated in the dark at room temperature for 1 h, and were centrifuged at 12 000×*g* for 10 min. The absorbance of supernatants was measured at 412 nm using a UV-vis spectrophotometer (Genesys 10uv, Thermo Scientific, USA) against a blank that consisted of phosphate buffer and Ellman's reagent. The SH content was calculated using the following equation:

$$\text{SH } (\mu\text{mol g}^{-1}) = (70.67 \times A_{412} \times D)/C$$

where A_{412} represents the absorbance at 412 nm, C represents the protein concentration of the dispersion (mg mL^{-1}), D represents the dilution factor, and the value of 70.67 is a constant calculated from $10^6/(1.415 \times 10^4)$, where 1.415×10^4 (M^{-1} cm^{-1}) is the molar extinction coefficient of DTNB in phosphate buffer.

2.3.6. Surface hydrophobicity. The surface hydrophobicity (H_0) was determined using the fluorescent probe 1-anilino-8-naphthalenesulfonate (ANS) following the method described by Kato and Nakai (1980)[47] with slight modifications. The samples were serially diluted to five concentrations ranging from 0.02% to 0.1% w/v using 0.01 M phosphate buffer (pH 7). For each measurement, 10 μL of ANS solution (8 mM in 0.01 M phosphate buffer, pH 7) was added to 2 mL of the diluted protein dispersion and incubated in the dark for 15 min at room temperature. The fluorescence intensity (FI) was measured using a fluorescence spectrophotometer (Fluostar Optima, BMG labtech, Germany) at an excitation wavelength of 355 nm and an emission wavelength of 492 nm. The buffer–ANS mixture was used as a blank for background correction. All FI measurements were performed in triplicate for each dilution, and H_0 was calculated from the slope of the linear regression curve plotting FI against protein concentration.

2.3.7. Sodium dodecyl sulfate-polyacrylamide gel electrophoresis (SDS-PAGE). The molecular weight distribution was investigated using SDS-PAGE based on the method described by Laemmli (1970)[48] with slight modifications. Samples were mixed with 2× Laemmli buffer (Bio-Rad, USA) at a 1 : 1 v/v ratio, with or without 5% v/v 2-mercaptoethanol (β-ME) for reducing and non-reducing conditions, respectively. All wells were loaded with 20 μL of protein samples containing 20 μg of total protein. A 10 μL aliquot of molecular weight protein standard (Precision Plus Protein Unstained Standards, 10–250 kDa, Bio-Rad, USA) was also included as a molecular weight marker. The electrophoresis was performed on a 4% stacking gel at 70 V and a 12% resolving gel at 100 V until the dye front reached the bottom (Mini-PROTEAN II, Bio-Rad, USA). After electrophoresis, the gels were fixed in a solution containing 50% (v/v) methanol and 10% (v/v) acetic acid for 45 min. Subsequently, the gels were stained overnight in Coomassie Brilliant Blue R-250 solution (0.05% w/v in 5% w/v acetic acid and 15% v/v methanol). Finally, the gels were destained with multiple rinses of deionised water until a clear background was obtained. Gel images were captured using an Azure imaging system (Azure 600, Azure Biosystems, USA).

2.3.8. Attenuated total reflectance-Fourier transform infrared (ATR-FTIR) spectroscopy. Infrared spectra were recorded using a FTIR spectrometer equipped with a single diamond ATR crystal (Spectrum 100, PerkinElmer, USA) following previous studies.[49,50] All spectra were acquired over 650–4000 cm^{-1} from 32 scans at 4 cm^{-1} resolution against the background. The original spectra were normalised and baseline corrected. To obtain the protein spectra, the buffer spectra, which were collected under the same settings, were subtracted from the sample spectra. To resolve the overlapping protein secondary structures in the amide I region (1600–1700 cm^{-1}), second derivative analysis was performed (OriginPro V2023, Origin Lab Corp., USA). The number of bands and their position were detected from the minima in the second derivative spectra of the amide I region after smoothing with a 9-point Savitsky–Golay function. Subsequently, peak fitting steps were performed using a Gaussian function. During the iteration process, the peak positions were fixed while the band widths and heights were allowed to adjust to the best fit. The relative content of each secondary structure components (α-helix, β-sheets, β-turns and random coils) was estimated from the relative areas of each resolved band to the total amide I area.

2.4. Gelling properties

2.4.1. Rheological properties. All rheological analyses were performed on a rheometer (HAAKE MARS III, Thermo Scientific, Germany) equipped with a 35 mm diameter parallel plate (Plate P35 TiL). Approximately 1 mL of 10% (w/v) MTG-treated BSFL protein dispersion was loaded onto the lower plate and the gap between the lower and upper plates was adjusted to 1 mm. All samples were equilibrated at 25 °C for 5 min before the measurements. To ensure that subsequent rheological analyses were performed within the linear viscoelastic region (LVR), a strain sweep test (0.01 to 100% strain at a frequency of 1 Hz and 25 °C) was performed on untreated BSFL protein dispersion to determine the LVR. The recorded data were processed using HAAKE RheoWin Data Manager (version 4.82).

A frequency sweep test was performed at a fixed strain of 1% in the range of 0.1–100 Hz at 25 °C. This strain level was selected based on preliminary strain sweep tests to ensure that measurements were conducted within the linear viscoelastic region (LVR). The log–log plot of storage modulus (G') as a function of angular frequency (ω) was fitted to the power-law model following Katzav *et al.* (2020):[51]

$$G' = k(\omega)^n$$

where ω is the angular frequency, k is the power law constant, and n represents the frequency exponent.

2.4.2. Water holding capacity (WHC). WHC of the BSFL protein dispersions (10% w/v) was determined using a centrifugation method adapted from Urbina *et al.* (2021)[52] with slight modifications. Approximately 1 g of sample was weighed and centrifuged at 635×*g* for 15 min at 4 °C using a microcentrifuge (5425R, Eppendorf, Germany). The liquid expelled from the gels

was decanted and the WHC was calculated based on the weight difference using the following:

$$\text{WHC (\%)} = [(W2 - W1)/W0] \times 100$$

where $W2$ is the weight of the centrifuge tube with sample after centrifugation (g), $W1$ is the weight of the centrifuge tube only (g) and $W0$ is the weight of the sample before centrifugation (g).

2.5. Statistical analysis

Each treatment was performed in three independent experimental replicates, with each replicate consisting of freshly prepared BSFL protein dispersions. Subsequently, all measurements were performed in technical triplicate for each independent sample preparation. The results were expressed as mean ± standard deviation (SD). The statistical analyses were performed using SPSS software (version 26.0; IBM SPSS Statistics, Chicago, IL, USA). Data normality and homogeneity of variance were assessed using the Shapiro–Wilk test and Levene's test, respectively. One-way ANOVA followed by Tukey's HSD post hoc test was applied to data that satisfied the assumptions of normality and homogeneity of variance. For data that violated these assumptions, the non-parametric Kruskal–Wallis test followed by Bonferroni-adjusted pairwise comparisons based on ranks was applied. Statistical significance was established at a 95% confidence interval ($p < 0.05$).

3 Results and discussion

3.1. Structural and physicochemical properties

3.1.1. Particle size and PdI. The *z*-average, which represents the intensity-based mean hydrodynamic particles size, of BSFL protein before and after MTG treatment for different durations is shown in Table 1. The *z*-average in the non-MTG control was the lowest and gradually increased with extended MTG incubation, reaching a significantly higher ($p < 0.05$) *z*-average compared to the control after 24 h of MTG treatment. This trend suggests the continuous formation of larger aggregates as a result of MTG crosslinking. To obtain a more comprehensive understanding on the effect of MTG on particle size, it is essential to interpret these results alongside other DLS parameters.

The PdI was further analysed to quantify the degree of particle size heterogeneity in the samples. A progressive increase in PdI with increasing MTG incubation time was observed, with significantly higher ($p < 0.05$) PdI recorded at 24 h as compared to the non-MTG control (Table 1). This result represents a broader particle size distribution in the MTG-treated BSFL protein dispersions after prolonged incubation time, arising from the emergence of either smaller or larger particles during the protein crosslinking process that increased the size variability. To elucidate the relative abundance of the different size populations in this polydisperse dispersions, volume-based particle size distribution was analysed.

As shown in Fig. 1, the control and MTG treated samples at 0.5 h, 1 h, 2 h and 4 h showed unimodal size distribution with peak values at 139.58, 147.30, 164.50, 170.03 and 168.53 nm, respectively. These results clearly revealed a shift of BSFL protein size populations towards larger diameters with increasing MTG incubation time. The progressive growth in particle size as incubation time increases owing to a higher degree of crosslinking is commonly observed in similar studies.[53,54]

As MTG incubation time extended to 20 h and 24 h, the particle size distribution shifted from a unimodal to a bimodal pattern. This transformation is consistent with the higher PdI reported earlier. Specifically, two distinct peak values were detected at 125.46 nm (67.2% area) and 170.2 nm (32.8% area) for the sample treated for 20 h. This distribution indicated the emergence of a new population of smaller particles alongside a reduction in the % area of the larger size peak. For the sample crosslinked for 24 h, a further reduction in the mean particle size of the first peak to 59.36 nm (49.7%) was observed, while the mean size of the second peak increased to 201.27 nm (58.7%). These results clearly demonstrated the size-reducing impact of MTG treatment once the incubation time exceeded a certain threshold. The compaction can be explained by the formation of intramolecular isopeptide bonds between residues within the same polypeptide chains, which draw the protein chains closer together and lead to the formation of smaller and more compact protein aggregates.[55]

Although smaller particles accounted for a large proportion of the volume, the fewer but larger particles may have scattered more light thereby skewing the intensity-weighted measurement toward a higher mean size. This effect explains the

Table 1 *Z*-average and PdI of BSFL protein dispersions after MTG treatment for different durations[a]

Incubation time	*z*-average (nm)	PdI
Non-MTG	133.96 ± 5.56^{a}	0.154 ± 0.006^{ab}
0.5 h	139.77 ± 8.72^{a}	0.148 ± 0.008^{a}
1 h	147.81 ± 9.36^{a}	0.168 ± 0.020^{ab}
2 h	149.05 ± 9.46^{a}	0.176 ± 0.044^{abc}
4 h	148.25 ± 9.35^{a}	0.179 ± 0.024^{abc}
20 h	145.60 ± 8.49^{a}	0.190 ± 0.044^{bc}
24 h	153.47 ± 3.94^{b}	0.214 ± 0.031^{c}

[a] Values are expressed as means ± SD from triplicate measurements. Different superscripts in the same column indicate significant differences ($p < 0.05$) between treatments.

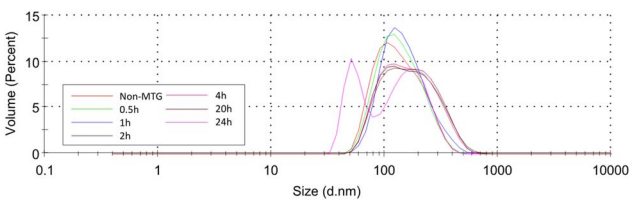

Fig. 1 Volume-based particle size distribution of BSFL protein dispersions after MTG treatment for different durations.

significantly higher *z*-average in the 24 h sample reported earlier.

3.1.2. Turbidity. Turbidity values were used as macroscopic indicators of protein aggregation. As shown in Table 2, the absorbance at both 400 and 600 nm followed similar trends to the particle size distributions; however the differences in turbidity among all samples were not statistically significant ($p > 0.05$). Generally, turbidity is associated with the particles size in the dispersion, where larger particles are able to scatter light more effectively and result in higher turbidity.[56] Despite shifts in particle size being detected in DLS analysis, the extent of these changes during MTG induced aggregation may be insufficient to markedly change light scattering intensity or significantly increase the turbidity. The results are attributable to the higher responsiveness of spectrophotometric turbidity measurements to large particle populations, while subtle shifts in particle size distribution or compaction may not generate measurable changes in light scattering intensity.[57]

3.1.3. Zeta potential. The effect of MTG treatment on the zeta potential of BSFL protein dispersions is shown in Table 3. The zeta potential of BSFL protein dispersions treated with MTG for different durations ranges from −23.26 mV to −27.69 mV. The absolute zeta potential values in the range of (±)20–30 mV for all samples conferred moderate colloidal stability to the protein dispersions even after prolonged MTG treatment.[58]

The results also showed that MTG crosslinking had minimal influence on the net surface charge distribution of the BSFL protein molecules regardless of the incubation time, as evidenced by the insignificant differences ($p > 0.05$) in zeta potential among all samples. This can also infer that electrostatic interactions did not play a major role in promoting aggregation of BSFL protein in the presence of MTG. Despite similar findings being reported in other protein systems,[59,60] opposing results have also been reported in the literature. For instance, the conversion of neutral glutamine residues to negatively charged glutamic acid during the MTG-catalysed deamidation reaction can increase the net negative charge of protein.[61] Since deamidation is generally a secondary MTG-catalysed reaction that takes place only under limited availability of amine donors like lysine, the present results indicate that crosslinking represented the primary reaction pathway in this study.

Table 3 Zeta potential of protein dispersions after MTG treatment for different durations[a]

Incubation time	Zeta potential (mV)
Non-MTG	−25.62 ± 1.57[a]
0.5 h	−26.60 ± 1.42[a]
1 h	−27.28 ± 2.14[a]
2 h	−27.69 ± 1.09[a]
4 h	−26.32 ± 1.48[a]
20 h	−23.26 ± 2.18[a]
24 h	−24.76 ± 2.30[a]

[a] Values are expressed as means ± SD from triplicate measurements. The same superscripts in the same column indicate no significant differences ($p > 0.05$) between treatments.

3.1.4. Free amino group content. As shown in Table 4, the non-MTG control exhibited the highest absorbance at 340 nm (Abs_{340nm}), establishing a baseline level of accessible free amino groups. A progressive decrease in Abs_{340nm} values was observed with increasing incubation time from 0.5 h to 24 h, with significantly lower ($p < 0.05$) Abs_{340nm} values at 24 h relative to the non-MTG control. The results implied the continuous depletion of free ε-amino groups on lysine residues due to the formation of MTG-catalysed G–L isopeptide bonds, thereby providing quantitative evidence for a progressive increase in the crosslinking degree. The corresponding degree of crosslinking, which is measured by the relative decrease in free amino groups compared to the non-MTG control, was found to increase from approximately 3.12% to 21.57% as the MTG crosslinking time increased from 0.5 h to 24 h (Table 4). The time-dependent reduction behaviour of free amino groups has also been reported for pea, soy and rapeseed proteins treated with MTG.[62–64]

3.1.5. Free and total SH group content. Table 5 shows the changes in both free and total SH contents in BSFL protein dispersions following MTG treatment for various incubation times, indicating MTG-induced structural modifications. The

Table 2 Turbidity of BSFL protein dispersions after MTG treatment for different durations[a]

Incubation time	Abs_{400}	Abs_{600}
Non-MTG	0.618 ± 0.005[a]	0.346 ± 0.015[a]
0.5 h	0.619 ± 0.042[a]	0.384 ± 0.060[a]
1 h	0.636 ± 0.041[a]	0.396 ± 0.049[a]
2 h	0.673 ± 0.014[a]	0.414 ± 0.074[a]
4 h	0.679 ± 0.032[a]	0.416 ± 0.083[a]
20 h	0.634 ± 0.012[a]	0.384 ± 0.070[a]
24 h	0.629 ± 0.043[a]	0.324 ± 0.074[a]

[a] Values are expressed as means ± SD from triplicate measurements. The same superscripts in the same column indicate no significant differences ($p > 0.05$) between treatments.

Table 4 Free amino group content (Abs_{340nm}) and the crosslinking degree of BSFL protein dispersions as a function of MTG incubation time[a]

Incubation time	Abs_{340nm}	Crosslinking degree (%)
Non-MTG	0.688 ± 0.043[b]	NA
0.5 h	0.666 ± 0.034[ab]	3.12
1 h	0.658 ± 0.042[ab]	4.28
2 h	0.647 ± 0.021[ab]	5.96
4 h	0.645 ± 0.041[ab]	6.12
20 h	0.618 ± 0.034[ab]	10.20
24 h	0.539 ± 0.088[a]	21.57

[a] Values are expressed as means ± SD from triplicate measurements. Different superscripts in the same column indicate significant differences ($p < 0.05$) between treatments.

Table 5 Free and total SH content of BSFL protein dispersions after MTG treatment for different durations[a]

Incubation time	Free SH (μmol g^{-1})	Total SH (μmol g^{-1})
Non-MTG	4.314 ± 0.357^{c}	6.105 ± 0.225^{b}
0.5 h	4.109 ± 0.296^{bc}	5.728 ± 0.284^{ab}
1 h	3.769 ± 0.224^{bc}	5.189 ± 0.467^{ab}
2 h	3.641 ± 0.208^{a}	4.977 ± 0.458^{a}
4 h	3.692 ± 0.152^{a}	5.047 ± 0.483^{a}
20 h	3.620 ± 0.144^{a}	5.080 ± 0.345^{a}
24 h	3.574 ± 0.099^{a}	5.026 ± 0.052^{a}

[a] Values are expressed as means ± SD from triplicate measurements. Different superscripts in the same column indicate significant differences ($p < 0.05$) between treatments.

Table 6 Surface hydrophobicity of BSFL protein dispersions after MTG treatment for different durations[a]

Incubation time	Surface hydrophobicity ($H_0 \times 10^2$)
Non-MTG	835.17 ± 27.61^{c}
0.5 h	814.69 ± 27.77^{c}
1 h	805.57 ± 13.01^{bc}
2 h	758.97 ± 32.57^{abc}
4 h	760.89 ± 38.80^{abc}
20 h	696.91 ± 29.84^{a}
24 h	728.50 ± 21.38^{ab}

[a] Values are expressed as means ± SD from triplicate measurements. Different superscripts in the same column indicate significant differences ($p < 0.05$) between treatments.

highest levels of free SH and total SH were found in the non-MTG control. With increasing MTG treatment duration, both free SH and total SH contents gradually declined, with significantly lower values ($p < 0.05$) recorded after 2 h compared to the control. Notably, the reduction in total SH was consistently greater than that of free SH, suggesting that SH groups buried within the protein structure participated in SS bond formation alongside free SH during the MTG treatment. A mechanistic explanation for this could be that the formation of isopeptide bonds, catalysed by MTG at accessible substrates on the protein surface, may promote protein conformational rearrangement and aggregation, indirectly increasing the proximity of SH groups. This facilitates greater SH–SH interactions and increases the chances of SS bond formation *via* oxidation of SH groups and/or SH/SS exchange reactions.[65,66] Such findings have similarly been reported for various protein systems, where MTG crosslinking resulted in protein conformational rearrangement beyond surface-level modification.[44,67,68]

However, both free and total SH contents remained insignificantly different ($p > 0.05$) during extended incubation from 2 h to 24 h. Since no additional denaturing agents were applied under the present experimental conditions, it is speculated that a substantial proportion of reactive SH groups capable of participating in SS bond formation had already reacted by 2 h. At longer incubation times, the formation of more rigid and compact aggregates likely restricted structural mobility, thereby limiting the ability of residual SH groups to undergo further oxidation. These factors may explain the plateau observed in both free SH and total SH contents. In line with the earlier free amino group content results, the absence of additional increases in SS bonds implies that SS bonds primarily contributed to the initial stages of network formation, while subsequent polymerisation of BSFL protein was likely supported by the MTG-catalysed isopeptide bonds.

3.1.6. Surface hydrophobicity. As shown in Table 6, the non-MTG control displayed the highest surface hydrophobicity (H_0) value followed by a decreasing trend as the incubation time increased. The H_0 values were significantly lower ($p < 0.05$) after 20 h and 24 h of MTG treatment as compared to the control. This reduction is consistent with previous studies, which reported that increasing crosslinking causes more hydrophobic residues to become buried within aggregates.[60,69] The extensive intra- and intermolecular crosslinks formed at longer incubation times impose greater steric hindrance that impedes the accessibility of ANS probe to the hydrophobic sites, leading to lower measured surface hydrophobicity.[65,70]

3.1.7. Protein molecular weight distribution. The SDS-PAGE patterns of MTG-treated BSFL proteins were examined under non-reducing and reducing conditions to gain insights into the MTG crosslinking mechanism and to distinguish the contribution of reducible SS bonds from that of non-reducible isopeptide bonds in stabilising the protein aggregates (Fig. 2). Under non-reducing conditions, several distinct bands were found in the non-MTG control sample (lane C) at approximately 75 kDa, 50 kDa, 37 kDa, and 25 kDa along with several bands of <20 kDa. The electrophoretic profile observed aligns with characteristic bands previously reported for BSFL protein.[71–74] Although several proteomic studies on BSFL protein are available, the identities of specific BSFL polypeptide subunits remain largely uncharacterised.[71,75] Hence, the present study primarily focuses on monitoring changes in electrophoretic patterns and molecular weight distribution without making definitive assignments regarding the identities of the individual protein bands.

Comparisons of the SDS-PAGE profiles of the non-MTG control and MTG-treated samples clearly revealed a similar overall molecular weight distribution between 15 and 250 kDa. However, the intensity of several bands changed noticeably with increasing MTG incubation time. Notably, the bands around 75 kDa, 37 kDa, and 25 kDa present in the control sample became nearly undetectable after 0.5 h of MTG treatment, while the <20 kDa bands gradually diminished over time. Concurrently, intense smearing dark bands of >250 kDa were detected on top of the resolving gels in all MTG treated samples. These observations indicated that crosslinking of lower molecular weight protein molecules had already occurred as early as 0.5 h of MTG treatment, leading to the formation of high molecular weight protein aggregates that were too large to enter the resolving gels. As these dark bands became more prominent in samples crosslinked for 1 h or longer, it suggests that a greater amount of these covalent aggregates was formed. Electrophoretic patterns revealing the time-dependent activity of MTG have

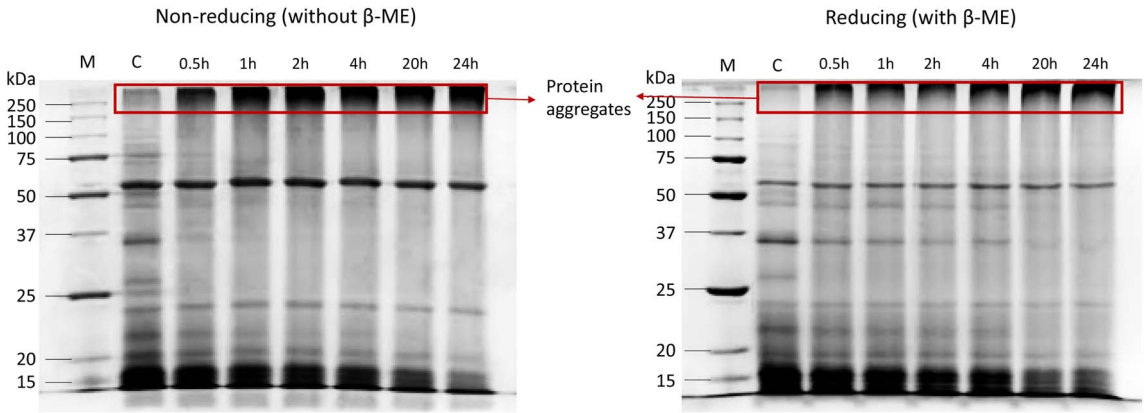

Fig. 2 Non-reducing and reducing SDS-PAGE of BSFL protein dispersions after MTG treatment for different durations. Lane M is the standard protein ladder and lane C is the control sample without MTG.

been reported for other proteins.[31,76] In SDS-PAGE observed for another insect protein system (*Protaetia brevitarsis* larvae), a slower decline in the intensity of the low molecular weight bands and the persistence of protein subunits at approximately 75 kDa were observed.[31] These variations in electrophoretic profiles highlight differences in susceptibility to MTG crosslinking and in the kinetics of aggregation compared with BSFL protein.

Clear differences were observed between electrophoretic patterns obtained under reducing and non-reducing conditions. The intense high molecular weight dark bands (>250 kDa) found in all MTG-treated samples appeared thinner under reducing conditions accompanied by an increase in the intensity of the lower molecular weight bands at approximately 37 kDa and <20 kDa. The 50 kDa band which was relatively thick under non-reducing conditions also became thinner after reduction. Since β-ME is a strong reducing agent that disrupts SS bonds, these shifts are probably due to the partial dissociation of high molecular weight aggregates into smaller protein fragments due to the cleavage of SS linkages. However, the persistence of dark bands at the top of the resolving gel even under reducing conditions indicates that a large proportion of aggregates were stabilised by non-reducible bonds, potentially including isopeptide bonds formed during MTG crosslinking. The evolution of electrophoretic patterns under both non-reducing and reducing SDS-PAGE collectively suggests that BSFL protein aggregates were stabilised through a combination of SS bonds and MTG-catalysed isopeptide bonds, although structural characterisation would be required to verify this interpretation.

3.1.8. Protein secondary structures. FTIR spectroscopy was employed to provide insights into the structural changes of BSFL protein during MTG crosslinking. The amide I region (1600–1700 cm^{-1}) of FTIR spectra, which mainly arises from C=O stretching vibrations of the peptide backbone, is the most structurally informative region to reveal secondary structure changes caused by MTG treatments. The amide I band position remained relatively constant at around 1637–1639 cm^{-1} across all samples, but its intensity was consistently higher in MTG-treated samples compared to the non-MTG control (Fig. S1). This suggests that MTG crosslinking induced rearrangements in the secondary structure.

More precisely, the relative proportions of α-helix, β-sheet, β-turn, and random coil structures as shown in Table 7 were quantified from the bands resolved in the second derivative spectra (Fig. S2). β-Sheets were found as the main secondary structure in all samples, which corroborates the findings of Xu *et al.* (2023).[77] Moreover, the results showed a significant increase ($p < 0.05$) in β-sheet content after 0.5 h of incubation compared to the non-MTG control. This was accompanied by a concomitant reduction in α-helix and β-turn contents, implying their conversion into β-sheet structures. These changes can be attributed to the formation of G–L isopeptide bonds, which caused perturbation of hydrogen bonds in the native α-helix and β-turn structures and promoted structural rearrangement into β-sheet-rich assemblies.[78,79] Consistent with previous studies, such β-sheet structures stabilised by intermolecular hydrogen bonds can develop into ordered, stable aggregates and protein networks with stronger mechanical strength.[80,81]

However, extending the incubation period beyond 0.5 h had minimal impact ($p > 0.05$) on the secondary structures up to 20 h. The relatively stable structural profile from 1 h to 20 h may be explained by the formation of isopeptide bonds that have restricted chain mobility and limited further conformational rearrangements.[54,82] In addition, the formation of SS bonds also imparted stability to the secondary structures,[83] consistent with the earlier findings from SH group content analysis. These results collectively suggested that secondary structure adjustments occur primarily during the early stages of crosslinking, while subsequent crosslinking serves to reinforce the existing protein network without significantly altering its secondary conformation.

Nevertheless, after 24 h of incubation, a significant increase ($p < 0.05$) in random coil content was observed, accompanied by a reduction in β-sheet content albeit insignificant ($p > 0.05$). This trend aligns with previous studies, which indicate that extensive crosslinking can partially destabilize ordered

Table 7 Composition of secondary structures of BSFL protein dispersions after MTG treatment for different durations[a]

Incubation time	β-Sheet %	Random coil %	α-Helix %	β-Turn %
Non-MTG	47.02 ± 0.53[a]	15.31 ± 0.58[a]	12.24 ± 1.74[a]	25.45 ± 1.80[a]
0.5 h	50.56 ± 0.94[b]	14.88 ± 0.53[a]	11.14 ± 1.66[a]	23.43 ± 1.76[a]
1 h	50.14 ± 0.75[b]	15.72 ± 1.11[ab]	11.55 ± 1.41[a]	22.60 ± 1.93[a]
2 h	50.61 ± 0.16[b]	14.66 ± 0.29[a]	10.66 ± 1.40[a]	24.06 ± 1.67[a]
4 h	51.49 ± 1.01[b]	15.54 ± 0.92[ab]	10.50 ± 2.15[a]	22.48 ± 2.08[a]
20 h	51.50 ± 0.30[b]	16.27 ± 0.48[ab]	10.23 ± 0.42[a]	22.01 ± 1.05[a]
24 h	50.07 ± 2.56[ab]	17.59 ± 1.40[b]	10.24 ± 2.33[a]	22.10 ± 2.58[a]

[a] Values are expressed as means ± SD from triplicate measurements. Different superscripts in the same column indicate significant differences ($p < 0.05$) between treatments.

structures by disrupting β-sheet stacking, resulting in more irregular conformations.[65,84]

3.2. Gelling properties

3.2.1. Frequency sweep. Fig. 3 shows the frequency sweep spectra of MTG-treated BSFL protein dispersions for different incubation times. The resulting frequency sweep spectra reflect the viscoelastic relaxation behaviour of BSFL protein gels over time, providing insights into their mechanical stability.

All samples exhibited increasing G' as the frequency increased from 0.1 Hz to 100 Hz, indicating frequency dependent behaviour. Nevertheless, differences in the slope of the spectra revealed differences in the degree of frequency dependence among the samples. Remarkably, the control and MTG-treated samples at 0.5 h, 1 h, 2 h and 4 h displayed steeper slopes whereas the samples treated for 20 h and 24 h displayed comparatively flatter slopes. Such rheological responses demonstrate that the G' values of the protein network formed after 20 h and 24 h of MTG treatment were less frequency dependent than those of the protein network formed during the earlier incubation periods.

The n and k values derived from the fitting of frequency sweep spectra into the power law model were used as quantitative parameters to complement the spectral observations, with n reflecting the frequency dependence of the protein network and k representing the overall gel strength (Table 8). A significantly lower ($p < 0.05$) n value was observed after 20 h and 24 h of treatment compared to the control. Since smaller n values closer to zero represent lower frequency dependence, this result coincides with the slope trends of the frequency sweep spectra presented earlier, suggesting a transition from a highly frequency dependent, viscous-dominant gel state ($n \approx 1$) in the non-MTG treated control ($n = 0.877$) to elastic-dominant stable gel structures capable of resisting deformation across the tested frequency range after 20 h ($n = 0.346$) and 24 h ($n = 0.423$) of MTG treatment. The enhanced mechanical stability in these samples was attributed to the accumulation of covalent isopeptide bonds formed by MTG over prolonged incubation. Being approximately 20 times stronger than non-covalent interactions, these covalent isopeptide linkages limit molecular rearrangements within the protein network, thereby reinforcing its resistance to deformation over a broad range of time scales.[85,86] However, it is worth noting that all MTG-catalysed BSFL protein networks behaved as weak gels, showing frequency-dependent viscoelasticity indicated by n values greater than zero.[87]

On the other hand, significantly higher ($p < 0.05$) k values were attained after 20 h and 24 h of MTG treatment compared to the control. Nevertheless, the k value of the 24 h sample was substantially lower ($p < 0.05$) than that of the 20 h sample. To

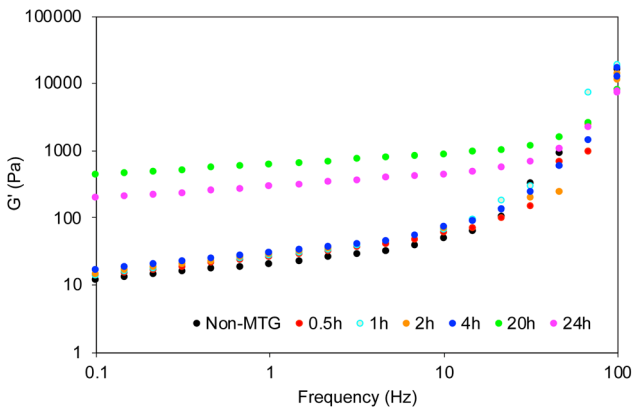

Fig. 3 Storage modulus (G') of BSFL protein gels as a function of frequency after MTG treatment for different durations.

Table 8 Power-law fitting parameters of BSFL protein gels obtained after MTG treatment for different durations[a]

Incubation time	Power law parameters		
	n	k (Pa·s^n)	R^2
Non-MTG	0.877 ± 0.156[b]	28.507 ± 5.688[a]	0.974
0.5 h	0.771 ± 0.056[b]	32.120 ± 4.629[a]	0.962
1 h	0.788 ± 0.063[b]	42.523 ± 2.607[a]	0.975
2 h	0.766 ± 0.039[b]	32.318 ± 4.190[a]	0.989
4 h	0.778 ± 0.024[b]	37.311 ± 7.977[a]	0.982
20 h	0.346 ± 0.080[a]	345.294 ± 2.943[c]	0.988
24 h	0.423 ± 0.067[a]	199.563 ± 22.051[b]	0.998

[a] Values are expressed as means ± SD from triplicate measurements. Different superscripts in the same column indicate significant differences ($p < 0.05$) between treatments. k is the power law constant and n is the frequency exponent.

facilitate a more direct comparison of the gel strength, G' values at a reference frequency of 1 Hz were analysed. The G' values continuously increased from 16 Pa in the untreated control to a maximum of 327 Pa after 20 h of MTG treatment, representing a 20-fold increase in the elastic magnitude. However, the G' values at 1 Hz declined to 185 Pa at 24 h. These changes suggest that while both treatments promoted stronger gel formation, the gel network began to weaken after 24 h. These observations highlighted that moderate crosslinking (around 10% crosslinking degree after 20 h; Table 4) produced the strongest and most stable BSFL protein network, whereas extensive crosslinking (around 21% crosslinking degree after 24 h; Table 4) compromised its structural integrity. Excessive isopeptide bond formation likely restricted chain mobility and obstructed optimal network assembly, leading to a more brittle gel with reduced elasticity.[88,89]

3.2.2. Water holding capacity (WHC). As shown in Table 9, the WHC of the MTG-catalysed BSFL protein network increased significantly ($p < 0.05$) by approximately threefold compared to the non-MTG control. The enhancement of WHC in MTG-treated samples aligns with findings from previous studies.[53,86,90] These studies suggested that MTG crosslinking promotes the formation of a gel network structure with stronger capillary forces, thereby allowing the gel matrix to retain more water. Additionally, higher WHC in the MTG-induced gel has also been associated with an increased amount of water tightly bound to protein macromolecules.[90] However, further studies on the distribution of water in different states are required to validate this explanation.

Interestingly, the highest WHC was recorded in the sample treated for 20 h, followed by a slight reduction in WHC from 91.51% to 87.14% after 24 h of MTG incubation. This indicates that a higher degree of crosslinking at prolonged incubation times does not necessarily improve the WHC of BSFL protein gels, but instead moderate crosslinking was more effective in retaining water within the gel network. A possible explanation for the slight reduction in WHC could be that extended MTG incubation altered the structural organisation of the gel network in a way that was less effective in water retention. Previous studies suggested that excessive crosslinking during prolonged incubation may hinder the uniform development of the protein network, rendering the entrapped water more easily expelled from the gel matrix.[53,81] However, further investigations should include microstructural analysis to validate this explanation.

Table 9 WHC of BSFL protein gels obtained after MTG treatment for different durations[a]

Incubation time	WHC (%)
Non-MTG	30.58 ± 2.65^{a}
0.5 h	81.15 ± 1.43^{b}
1 h	85.02 ± 4.59^{bc}
2 h	85.81 ± 4.20^{bc}
4 h	89.57 ± 1.02^{c}
20 h	91.51 ± 1.82^{c}
24 h	87.14 ± 1.71^{bc}

[a] Values are expressed as means ± SD from triplicate measurements. Different superscripts in the same column indicate significant differences ($p < 0.05$) between treatments.

3.3. Proposed mechanism of gelation

By synthesizing the findings of this study, a multi-stage mechanism is proposed to explain the influence of MTG incubation time on the gelation behaviour of BSFL protein. Overall, the gelation process follows a series of time-dependent transitions in the structural and physicochemical properties of the protein that affect its functionality.

During the early stage of MTG treatment (0.5–4 h), BSFL protein aggregates formed rapidly, as evidenced by the increase in particle size and formation of high molecular weight polymers in SDS-PAGE. The reduction in free amino group content confirmed the occurrence of MTG-catalysed crosslinking, obtaining approximately 3–6% crosslinking degree within this period. Simultaneously, FTIR results further revealed an increase in β-sheet content as early as 0.5 h, indicating that MTG treatment had induced intermolecular protein–protein interactions and structural reorganisation into stable secondary structures. The intermolecular hydrogen bonding between segments of β-sheet structures may serve as junction zones connecting protein molecules into the gel network with enhanced viscoelastic properties and WHC, which align with the findings from the current study.[91,92] Concurrently, the progressive MTG crosslinking process may have also drawn the SH groups closer and promoted SS bonds formation, as evidenced by the significant reduction in free and total SH contents after 2 h. While the MTG-catalysed ε-(γ-glutamyl)–lysine isopeptide bonds are expected to constitute the primary scaffold of the network, the SS bonds may have acted together to further densify and stabilise the protein network through additional covalent crosslinks. Both strong covalent bonds likely acted as fixatives of the protein network, collectively enhancing the protein network rigidity and resistance to deformation. Beyond 2 h, SS bond formation plateaued, possibly due to conformational constraints limiting further SH interactions. This shifted the mechanism of further aggregation of BSFL protein to one driven mainly by MTG-catalysed crosslinking.

At prolonged incubation times (20–24 h), the crosslinking degree increased to approximately 10–21%, leading to substantial structural reorganisation. The particle size distribution shifted from unimodal to bimodal, with a new population of smaller, compact aggregates alongside previously formed larger aggregates. The emergence of these smaller aggregates may be attributed to increased intramolecular crosslinking that potentially causing proteins to fold more compactly.[55]

At the 20 h mark, the gel exhibited the lowest frequency dependency (n value), the highest elasticity (k value) and the highest WHC compared to other incubation times. These results suggest that 20 h of MTG incubation was favourable for the development of a gel network that is sufficiently rigid to

resist frequency-dependent deformation yet flexible enough for elastic recovery under stress, while also being able to retain water within the matrix against centrifugal force. Based on previous studies, it is speculated that the bimodal size distribution at 20 h potentially enhanced the connectivity between aggregates, which could contribute to improved mechanical properties and WHC of protein gels.[93,94] However, the precise network architecture underlying these functional outcomes requires further confirmation through microstructural analysis.

At 24 h, despite achieving the highest degree of crosslinking (21%), the resulting gel exhibited reduced gel strength and WHC compared to 20 h. This indicates that prolonged MTG incubation for 24 h had potentially caused the network to become too rigid and brittle, lacking the flexibility necessary for elastic deformation, thereby leading to diminishing mechanical strength. Notably, the increased random coil content accompanied by a reduction in β-sheet content suggests that excessive crosslinks partially disrupted the ordered secondary structure. It is proposed that this conformational change compromised the regularity of the gel network and weakened the contribution of hydrogen bonding to the structural integrity. Furthermore, the presence of overly compact and small aggregates at 24 h potentially disrupted the optimal balance between large and small aggregates established at 20 h, which in turn could influence the continuity and uniformity of the network in a manner that is more susceptible to deformation and syneresis. Hence, these findings demonstrated that 20 h represents the optimal MTG incubation time under the conditions applied in this study, achieving crosslinking density and structural organisation that maximise both mechanical strength and WHC of the resultant gel.

4 Conclusions

This study systematically investigated the effects of MTG crosslinking on the structural, physicochemical, and gelling properties of BSFL protein. The extension of MTG incubation time promoted aggregate growth but prolonged incubation (20–24 h) resulted in the emergence of smaller particle populations, indicating structural compaction within aggregates. Longer incubation also increased the formation of isopeptide bonds, yielding a higher level of crosslinking. The maximal crosslinking degree of approximately 21.6% was attained after 24 h. Changes in SH content and surface hydrophobicity suggested that MTG-catalysed crosslinking induced structural modifications, and that SS bonds and hydrophobic interactions contributed to network stability. Secondary structure analysis showed that structural reorganization into β-sheet-rich conformations occurred within 0.5 h of incubation, whereas extended treatment primarily reinforced the existing structure through targeted crosslinking rather than extensive secondary structural changes. Functionally, MTG treatment significantly improved the gel strength after 20 h and 24 h of incubation, producing more solid-like weak gels with high WHC. The greatest gel strength was observed at 20 h, after which the gel structure began to weaken at 24 h, highlighting the time-dependent nature of the MTG-mediated gelling mechanism. These findings provide new mechanistic insights into how BSFL protein undergoes structural modifications, aggregation and gelation upon application of MTG. They also provide a scientific basis for the future development of BSFL-based texturized food products.

It should be noted that residual non-protein components including lipids and carbohydrates like chitin in the BSFL protein concentrate may influence gelation behaviour and WHC. Although these components do not directly participate in protein crosslinking, they may act as passive fillers and interfere with protein–protein interactions. As the investigation of their specific effects was beyond the scope of the present study, future work employing highly purified BSFL protein isolates is recommended to decouple the contributions of these non-protein components.

Author contributions

Xin Yun Chia: investigation, conceptualisation, writing – original draft, formal analysis, visualization. Siau Hui Mah: supervision, project administration, resources, writing – review and editing. Yun Ping Neo: supervision, conceptualisation, project administration, funding acquisition, writing – review and editing.

Conflicts of interest

There are no conflicts to declare.

Data availability

The data supporting this article have been included in this article and in the supplementary information (SI). Supplementary information is available. See DOI: https://doi.org/10.1039/d5fb00795j.

Acknowledgements

This work was funded by the Fundamental Research Grant Scheme (FRGS/1/2021/WAB04/TAYLOR/02/1), Ministry of Higher Education Malaysia. This work was supported by Taylor's University through its TAYLOR'S RESEARCH SCHOLARSHIP Programme.

References

1 I. B. Pam, L. Senaratne-Lenagala, A. Stube and A. Brackenridge, Protein demand: review of plant and animal proteins used in alternative protein product development and production, *Anim. Front.*, 2020, **10**, 53–63.
2 P. Wood and M. Tavan, A review of the alternative protein industry, *Curr. Opin. Food Sci.*, 2022, **47**, 100869.
3 N. M. de Carvalho, A. R. Madureira and M. E. Pintado, The potential of insects as food sources – a review, *Crit. Rev. Food Sci. Nutr.*, 2019, **60**, 3642–3652.

4 J. De Souza-Vilela, N. R. Andrew and I. Ruhnke, Insect protein in animal nutrition, *Anim. Prod. Sci.*, 2019, **59**, 2029–2036.
5 H. Čičková, G. L. Newton, R. C. Lacy and M. Kozánek, The use of fly larvae for organic waste treatment, *Waste Manag.*, 2015, **35**, 68–80.
6 D. G. A. B. Oonincx, S. Van Broekhoven, A. Van Huis and J. J. A. Van Loon, Feed conversion, survival and development, and composition of four insect species on diets composed of food by-products, *PLoS One*, 2015, **10**, 1–20.
7 J. M. Wilkinson, Re-defining efficiency of feed use by livestock, *Animal*, 2011, **5**, 1014–1022.
8 Y.-S. Wang and M. Shelomi, Review of black soldier fly (Hermetia illucens) as animal feed and human food, *Foods*, 2017, **6**, 1–23.
9 C. Huang, W. Feng, J. Xiong, T. Wang, W. Wang, C. Wang and F. Yang, Impact of drying method on the nutritional value of the edible insect protein from black soldier fly (Hermetia illucens L.) larvae: amino acid composition, nutritional value evaluation, in vitro digestibility, and thermal properties, *Eur. Food Res. Technol.*, 2019, **245**, 11–21.
10 V. V. Mshayisa, J. Van Wyk and B. Zozo, Nutritional, techno-functional and structural properties of black soldier fly (Hermetia illucens) larvae flours and protein concentrates, *Foods*, 2022, **11**, 724.
11 B. K. Mintah, R. He, A. A. Agyekum, M. Dabbour, M. K. Golly and H. Ma, Edible insect protein for food applications: Extraction, composition, and functional properties, *J. Food Process. Eng.*, 2020, **43**, 1–12.
12 L. W. Bessa, E. Pieterse, G. Sigge and L. C. Hoffman, An exploratory study into the use of black soldier fly (Hermetia illucens) larvae in the production of a vienna-style sausage, *Meat Muscle Biol.*, 2019, **3**, 289–298.
13 G. Siqueira, G. Novo, E. C. Tondo, R. Cruz, S. Thys and F. Cladera-Olivera, Production of protein-enriched bread through the incorporation of the black soldier fly (Hermetia illucens) larvae, *Food Sci. Technol.*, 2024, **44**, 1–9.
14 L. Miron, G. Montevecchi, L. I. Macavei, L. Maistrello, A. Antonelli and M. Thomas, Effect of black soldier fly larvae protein on the texture of meat analogues, *LWT–Food Sci. Technol.*, 2023, **181**, 114745.
15 A. Hidalgo, M. Cullere, A. Dalle Zotte and G. Pasini, Salt-soluble protein extracts from Hermetia illucens and Bombyx mori for high protein pasta production, *LWT–Food Sci. Technol.*, 2023, **190**, 115507.
16 B. Lamsal, H. Wang, P. Pinsirodom and A. T. Dossey, Applications of insect-derived protein ingredients in food and feed industry, *J. Am. Oil Chem. Soc.*, 2019, **96**, 105–123.
17 A. Gravel and A. Doyen, The use of edible insect proteins in food: Challenges and issues related to their functional properties, *Innovative Food Sci. Emerging Technol.*, 2020, **59**, 102272.
18 L. W. Bessa, E. Pieterse, J. Marais and L. C. Hoffman, Why for feed and not for human consumption? The black soldier fly larvae, *Compr. Rev. Food Sci. Food Saf.*, 2020, **19**, 2747–2763.
19 L. W. Bessa, E. Pieterse, J. Marais and L. C. Hoffman, Techno-functional properties of black soldier fly (Hermetia illucens) larvae, *J. Insects Food Feed*, 2022, **8**, 1047–1059.
20 S. Kumar, L. S. Queiroz, R. Marie, L. G. L. Nascimento, M. A. Mohammadifar, A. F. de Carvalho, C. M. C. Brouzes, H. Fallquist, W. Fraihi and F. Casanova, Gelling properties of black soldier fly (Hermetia illucens) larvae protein after ultrasound treatment, *Food Chem.*, 2022, **386**, 132826.
21 J. Buchert, D. E. Cura, H. Ma, C. Gasparetti, E. Monogioudi, G. Faccio, M. Mattinen, H. Boer, R. Partanen, E. Selinheimo, R. Lantto and K. Kruus, Crosslinking food proteins for improved functionality, *Annu. Rev. Food Sci. Technol.*, 2010, **1**, 113–138.
22 H. Ando, M. Adachi, K. Umeda, A. Matsuura, M. Nonaka, R. Uchio, H. Tanaka and M. Motoki, Purification and characteristics of a novel transglutaminase derived from microorganisms, *Agric. Biol. Chem.*, 1989, **53**, 2613–2617.
23 K. Yokoyama, N. Nio and Y. Kikuchi, Properties and applications of microbial transglutaminase, *Appl. Microbiol. Biotechnol.*, 2004, **64**, 447–454.
24 A. M. Ahhmed, R. Kuroda, S. Kawahara, K. Ohta, K. Nakade, T. Aoki and M. Muguruma, Dependence of microbial transglutaminase on meat type in myofibrillar proteins cross-linking, *Food Chem.*, 2009, **112**, 354–361.
25 A. M. Herrero, M. I. Cambero, J. A. Ordóñez, L. de la Hoz and P. Carmona, Raman spectroscopy study of the structural effect of microbial transglutaminase on meat systems and its relationship with textural characteristics, *Food Chem.*, 2008, **109**, 25–32.
26 T. Şanli, E. Sezgin, O. Deveci, E. Şenel and M. Benli, Effect of using transglutaminase on physical, chemical and sensory properties of set-type yoghurt, *Food Hydrocoll.*, 2011, **25**, 1477–1481.
27 S. Chanarat, S. Benjakul and A. H-Kittikun, Comparative study on protein cross-linking and gel enhancing effect of microbial transglutaminase on surimi from different fish, *J. Sci. Food Agric.*, 2012, **92**, 844–852.
28 S. B. M. Yasir, K. H. Sutton, M. P. Newberry, N. R. Andrews and J. A. Gerrard, The impact of transglutaminase on soy proteins and tofu texture, *Food Chem.*, 2007, **104**, 1491–1501.
29 W. Q. Wang, L. W. Zhang, H. Xue and L. Yi, Cheese whey protein recovery by ultrafiltration through transglutaminase (TG) catalysis whey protein cross-linking, *Food Chem.*, 2017, **215**, 31–40.
30 X. Zhao, J. L. Vázquez-Gutiérrez, D. P. Johansson, R. Landberg and M. Langton, Yellow mealworm protein for food purposes – extraction and functional properties, *PLoS One*, 2016, **11**, e0147791.
31 T. K. Kim, H. I. Yong, H. W. Jang, Y. B. Kim and Y. S. Choi, Functional properties of extracted protein from edible insect larvae and their interaction with transglutaminase, *Foods*, 2020, **9**, 1–11.
32 H. K. Ravi, A. Degrou, J. Costil, C. Trespeuch, F. Chemat and M. A. Vian, Effect of devitalization techniques on the lipid, protein, antioxidant, and chitin fractions of black soldier fly (Hermetia illucens) larvae, *Eur. Food Res. Technol.*, 2020, **246**, 2549–2568.

33 X. Y. Chia, H. T. Peng, S. H. Mah, Y. H. Kuan, B. T. Z. Wong and Y. P. Neo, Heat-induced gelation of black soldier fly larvae (Hermetia illucens) protein: aggregation and rheological characterization, *Eur. Food Res. Technol.*, 2025, **251**, 135–150.
34 C. M. Beliciu and C. I. Moraru, The effect of protein concentration and heat treatment temperature on micellar casein–soy protein mixtures, *Food Hydrocoll.*, 2011, **25**, 1448–1460.
35 G. A. Ruiz, W. Xiao, M. Van Boekel, M. Minor and M. Stieger, Effect of extraction pH on heat-induced aggregation, gelation and microstructure of protein isolate from quinoa (Chenopodium quinoa Willd), *Food Chem.*, 2016, **209**, 203–210.
36 M. Nieuwland, W. G. Bouwman, L. Pouvreau, A. H. Martin and H. H. J. de Jongh, Relating water holding of ovalbumin gels to aggregate structure, *Food Hydrocoll.*, 2016, **52**, 87–94.
37 C. H. Tang, H. Wu, H. P. Yu, L. Li, Z. Chen and X. Q. Yang, Coagulation and gelation of soy protein isolates induced by microbial transglutaminase, *J. Food Biochem.*, 2006, **30**, 35–55.
38 Y. H. Zhang, C. H. Tang, Q. B. Wen, X. Q. Yang, L. Li and W. L. Deng, Thermal aggregation and gelation of kidney bean (Phaseolus vulgaris L.) protein isolate at pH 2.0: Influence of ionic strength, *Food Hydrocoll.*, 2010, **24**, 266–274.
39 S. H. Moon and S. J. Cho, Effect of microbial transglutaminase treatment on the techno-functional properties of mung bean protein isolate, *Foods*, 2023, **12**, 1998.
40 N. Raak, R. A. Abbate, M. Alkhalaf, A. Lederer, H. Rohm and D. Jaros, Concentration-triggered liquid-to-solid transition of sodium caseinate suspensions as a function of temperature and enzymatic cross-linking, *Food Hydrocoll.*, 2020, **101**, 105464.
41 D. Jaros, U. Schwarzenbolz, N. Raak, J. Löbner, T. Henle and H. Rohm, Cross-linking with microbial transglutaminase: Relationship between polymerisation degree and stiffness of acid casein gels, *Int. Dairy J.*, 2014, **38**, 174–178.
42 C. Y. Gan, L. H. Cheng and A. M. Easa, Physicochemical properties and microstructures of soy protein isolate gels produced using combined cross-linking treatments of microbial transglutaminase and Maillard cross-linking, *Food Res. Int.*, 2008, **41**, 600–605.
43 K. N. Ryan, B. Vardhanabhuti, D. P. Jaramillo, J. H. van Zanten, J. N. Coupland and E. A. Foegeding, Stability and mechanism of whey protein soluble aggregates thermally treated with salts, *Food Hydrocoll.*, 2012, **27**, 411–420.
44 X. Hu, W. K. Amakye, P. He, M. Wang and J. Ren, Effects of microfluidization and transglutaminase cross-linking on the conformations and functional properties of arachin and conarachin in peanut, *LWT–Food Sci. Technol.*, 2021, **146**, 111438.
45 T. Beveridge, S. Toma and S. Nakai, Determination of SH- and SS-groups in some food proteins using ellman's reagent, *J. Food Sci.*, 1974, **39**, 49–51.
46 X. Shen, T. Fang, F. Gao and M. Guo, Effects of ultrasound treatment on physicochemical and emulsifying properties of whey proteins pre- and post-thermal aggregation, *Food Hydrocoll.*, 2017, **63**, 668–676.
47 A. Kato and S. Nakai, Hydrophobicity determined by a fluorescence probe method and its correlation with surface properties of proteins, *Biochim. Biophys. Acta, Protein Struct.*, 1980, **624**, 13–20.
48 U. K. Laemmli, Cleavage of structural proteins during the assembly of the head of bacteriophage T4, *Nature*, 1970, **227**, 680–685.
49 D. Bogahawaththa, N. H. Bao Chau, J. Trivedi, M. Dissanayake and T. Vasiljevic, Impact of selected process parameters on solubility and heat stability of pea protein isolate, *LWT–Food Sci. Technol.*, 2019, **102**, 246–253.
50 A. Sadat and I. J. Joye, Peak fitting applied to fourier transform infrared and raman spectroscopic analysis of proteins, *Appl. Sci.*, 2020, **10**, 5918.
51 H. Katzav, L. Chirug, Z. Okun, M. Davidovich-Pinhas and A. Shpigelman, Comparison of thermal and high-pressure gelation of potato protein isolates, *Foods*, 2020, **9**, 1041.
52 P. Urbina, C. Marin, T. Sanz, D. Rodrigo and A. Martinez, Effect of HHP, enzymes and gelatin on physicochemical factors of gels made by using protein isolated from common cricket (Acheta domesticus), *Foods*, 2021, **10**, 858.
53 T. Hui and G. Xing, Effect of transglutaminase pre-crosslinking treatment incorporated with glucono-δ-lactone on the physicochemical and digestive properties of tofu, *Polymers*, 2022, **14**, 2364.
54 C. Wu, Y. Zhang, J. Wang, W. Xu, Z. Hu and C. Hu, Continuous enzyme crosslinking modifying colloidal particle characteristics and interface properties of rice bran protein to improve the foaming properties, *LWT–Food Sci. Technol.*, 2023, **184**, 114997.
55 A. Djoullah, G. Krechiche, F. Husson and R. Saurel, Size measuring techniques as tool to monitor pea proteins intramolecular crosslinking by transglutaminase treatment, *Food Chem.*, 2016, **190**, 197–200.
56 G. C. Jeffrey and R. H. Ottewill, Reversible aggregation Part I. Reversible flocculation monitored by turbidity measurements, *Colloid Polym. Sci.*, 1988, **266**, 173–179.
57 R. Esfandiary and C. R. Middaugh, in Ultraviolet absorption spectroscopy, *Analysis of Aggregates and Particles in Protein Pharmaceuticals*, ed. H.-C. Mahler, W. Jiskoot, John Wiley & Sons, Ltd, New Jersey, 2012, pp. 169–200.
58 C. Cano-Sarmiento, D. I. Téllez-Medina, R. Viveros-Contreras, M. Cornejo-Mazón, C. Y. Figueroa-Hernández, E. García-Armenta, L. Alamilla-Beltrán, H. S. García and G. F. Gutiérrez-López, Zeta potential of food matrices, *Food Eng. Rev.*, 2018, **10**, 113–138.
59 T. Zhang, Y. Zhao, X. Tian, J. Liu, H. Ye and X. Shen, Effect of ultrasound pretreatment on structural, physicochemical, rheological and gelation properties of transglutaminase cross-linked whey protein soluble aggregates, *Ultrason. Sonochem.*, 2021, **74**, 105553.
60 K. Kaczynska, A. G. B. Wouters and J. A. Delcour, Microbial transglutaminase induced modification of wheat gliadin

based nanoparticles and its impact on their air-water interfacial properties, *Food Hydrocoll.*, 2022, **127**, 107471.
61 A. L. C. Gaspar and S. P. De Góes-Favoni, Action of microbial transglutaminase (MTGase) in the modification of food proteins: A review, *Food Chem.*, 2015, **171**, 315–322.
62 A. Djoullah, F. Husson and R. Saurel, Gelation behaviors of denaturated pea albumin and globulin fractions during transglutaminase treatment, *Food Hydrocoll.*, 2018, **77**, 636–645.
63 S. Lu, W. Xiong, Y. Yao, J. Zhang and L. Wang, Investigating the physicochemical properties and air-water interface adsorption behavior of transglutaminase-crosslinking rapeseed protein isolate, *Food Res. Int.*, 2023, **174**, 113505.
64 C. Schäfer, C. Zacherl, K. H. Engel, S. Neidhart and R. Carle, Comparative study of gelation and cross-link formation during enzymatic exturization of leguminous proteins, *Innovative Food Sci. Emerging Technol.*, 2007, **8**, 269–278.
65 X. Ding, N. Zeng, G. Zhang, J. Pan, X. Hu and D. Gong, Influence of transglutaminase-assisted ultrasound treatment on the structure and functional properties of soy protein isolate, *J. Food Process. Preserv.*, 2019, **43**, e14203.
66 Y. Shi, T. Tang, T. Hui, Y. Chang, X. Chen and G. Xing, Effect of transglutaminase crosslinking on the protein structure and potential allergenicity of dual-protein system, with a focus on β-conglycinin, *LWT–Food Sci. Technol.*, 2023, **188**, 115417.
67 X. Chen, X. Zhu, F. Ning, S. Wang and Q. Zhao, Effect of transglutaminase-mediated cross-linking on physicochemical properties and structural modifications of rice dreg protein, *Foods*, 2025, **14**, 3719.
68 L. Fang, X. Han, Y. Zhang, T. Hui, L. Ding, W. Dai, Y. Han, M. Zheng and G. Xing, Does transglutaminase crosslinking reduce the antibody recognition capacity of β-lactoglobulin: An analysis from conformational perspective, *Molecules*, 2025, **30**, 685.
69 X. Zhou, Y. Zheng, Y. Zhong, D. Wang and Y. Deng, Casein-hempseed protein complex via cross-link catalyzed by transglutaminase for improving structural, rheological, emulsifying and gelation properties, *Food Chem.*, 2022, **383**, 132366.
70 S. Ganesh, D. W. Ningtyas and S. Prakash, Investigating the functionality of enzymatically (transglutaminase and alcalase) treated almond protein isolate, *Food Biosci.*, 2022, **49**, 101914.
71 M. G. Bonomini, B. Prandi and A. Caligiani, Black soldier fly (Hermetia illucens L.) whole and fractionated larvae: In vitro protein digestibility and effect of lipid and chitin removal, *Food Res. Int.*, 2024, **196**, 115102.
72 G. Leni, T. Tedeschi, A. Faccini, F. Pratesi, C. Folli, I. Puxeddu, P. Migliorini, N. Gianotten, J. Jacobs, S. Depraetere, A. Caligiani and S. Sforza, Shotgun proteomics, in-silico evaluation and immunoblotting assays for allergenicity assessment of lesser mealworm, black soldier fly and their protein hydrolysates, *Sci. Rep.*, 2020, **10**, 1228.
73 L. T. Miron, R. P. Postma, G. Bosch and M. H. M. Eppink, Preliminary evaluation of aqueous protein extraction from black soldier fly larvae (Hermetia illucens L.), *Ind. Biotechnol.*, 2019, **15**, 365–369.
74 L. S. Queiroz, M. Regnard, F. Jessen, M. A. Mohammadifar, J. J. Sloth, H. O. Petersen, F. Ajalloueian, C. M. C. Brouzes, W. Fraihi, H. Fallquist, A. F. de Carvalho and F. Casanova, Physico-chemical and colloidal properties of protein extracted from black soldier fly (Hermetia illucens) larvae, *Int. J. Biol. Macromol.*, 2021, **186**, 714–723.
75 V. Rabani, H. Cheatsazan and S. Davani, Proteomics and lipidomics of black soldier fly (Diptera: Stratiomyidae) and blow fly (Diptera: Calliphoridae) larvae, *J. Insect Sci.*, 2019, **19**, 1–9.
76 C. V. L. Giosafatto, N. M. Rigby, N. Wellner, M. Ridout, F. Husband and A. R. Mackie, Microbial transglutaminase-mediated modification of ovalbumin, *Food Hydrocoll.*, 2012, **26**, 261–267.
77 J. H. Xu, S. Xiao, J. H. Wang, B. Wang, Y. X. Cai and W. F. Hu, Comparative study of the effects of ultrasound-assisted alkaline extraction on black soldier fly (Hermetia illucens) larvae protein: Nutritional, structural, and functional properties, *Ultrason. Sonochem.*, 2023, **101**, 106662.
78 K. D. Mattice and A. G. Marangoni, Physical properties of zein networks treated with microbial transglutaminase, *Food Chem.*, 2021, **338**, 128010.
79 Y. Wang, K. Yu, Y. Xu, L. Guo and X. F. Du, Physicochemical properties of soya bean protein gel prepared by microbial transglutaminase in the presence of okara, *Int. J. Food Sci. Technol.*, 2015, **50**, 2402–2410.
80 B. P. Yaputri, S. Feyzi and B. P. Ismail, Transglutaminase-Induced Polymerization of Pea and Chickpea Protein to Enhance Functionality, *Gels*, 2024, **10**, 11.
81 Y. An, S. Xiong, R. Liu, J. You, T. Yin and Y. Hu, The effect of cross-linking degree on physicochemical properties of surimi gel as affected by MTGase, *J. Sci. Food Agric.*, 2021, **101**, 6228–6238.
82 J. Xu, L. Yang, Y. Nie, M. Yang, W. Wu, Z. Wang, X. Wang and J. Zhong, Effect of transglutaminase crosslinking on the structural, physicochemical, functional, and emulsion stabilization properties of three types of gelatins, *LWT–Food Sci. Technol.*, 2022, **163**, 113543.
83 Y. Chen, D. J. McClements, K. He, Z. Zhang, R. Zhang, J. Zhao, Z. Jin and L. Chen, Effect of transglutaminase on the structure, properties and oil absorption of wheat flour, *Food Chem.*, 2025, **463**, 141117.
84 W. Zhang, P. Zhao, J. Li, X. Wang, J. Hou and Z. Jiang, Effects of ultrasound synergized with microwave on structure and functional properties of transglutaminase-crosslinked whey protein isolate, *Ultrason. Sonochem.*, 2022, **83**, 105935.
85 F. Alavi, Z. Emam-Djomeh, M. Salami and M. Mohammadian, Effect of microbial transglutaminase on the mechanical properties and microstructure of acid-induced gels and emulsion gels produced from thermal denatured egg white proteins, *Int. J. Biol. Macromol.*, 2020, **153**, 523–532.
86 Y. Liu, Y. Liu, Z. Xu, M. Shan, X. Ge, Y. Zhang, S. Shao, L. Huang, W. Wang and F. Lu, Effects of Bacillus subtilis

transglutaminase treatment on the functional properties of whey protein, *LWT–Food Sci. Technol.*, 2019, **116**, 108559.
87 H. Kazazi, F. Khodaiyan, K. Rezaei, M. Pishvaei, M. A. Mohammadifar and S. Moieni, Rheology and microstructure of kefiran and whey protein mixed gels, *J. Food. Sci. Technol.*, 2017, **54**, 1168–1174.
88 H. Babin and E. Dickinson, Influence of transglutaminase treatment on the thermoreversible gelation of gelatin, *Food Hydrocoll.*, 2001, **15**, 271–276.
89 C. Liu, J. Song, L. Wang, P. Wang, J. Ma, B. Zhao, X. Chen, Y. Wang, W. Zhang and P. Wen, The impacts of different modification techniques on the gel properties and structural characteristics of fish gelatin, *Food Hydrocoll.*, 2025, **158**, 110536.
90 Y. Ouyang, J. Xu, F. Ji, M. Tan, S. Luo, X. Zhong and Z. Zheng, Properties of transglutaminase-induced myofibrillar/wheat gluten gels, *J. Food Sci.*, 2021, **86**, 2387–2397.
91 S. Damodaran, in Food proteins: an overview, in ed. S. Damodaran and A. Paraf, *Food Proteins and Their Applications*, Marcel Dekker, New York, 1997, pp. 1–24.
92 B. Lu, Z. Wang, N. Xiao, S. Guo and M. Ai, Enhancing beef mince gel strength and water-holding capacity: the concentration effect of sarcoplasmic protein, *Food Sci. Anim. Prod.*, 2026, **4**, 9240157.
93 A. Feichtinger, A. Jarray, W. G. Bouwman, C. P. Duif, M. C. Valverde-Ayllon, K. Heerkens, *et al.*, Biopolymer-based capillary suspensions: Influence of particle properties on network formation, *Food Hydrocoll.*, 2025, **163**, 111061.
94 A. J. Gravelle and A. G. Marangoni, Effect of matrix architecture on the elastic behavior of an emulsion-filled polymer gel, *Food Hydrocoll.*, 2021, **119**, 106875.